Journal of Nuclear Materials xxx (2011) xxx–xxx

Contents lists available at ScienceDirect

Journal of Nuclear Materials

journal homepage: www.elsevier.com/locate/jnucmat

Physical and chemical erosion studies of lithiated ATJ graphite ☆

V. Surla *, P. Raman, D. Burns, M.J. Neumann, D.N. Ruzic

Center for Plasma-Material Interactions, Department of Nuclear, Plasma and Radiological Engineering, University of Illinois at Urbana Champaign, Urbana, IL 61801, USA

ARTICLE INFO

Article history:
Available online xxxx

ABSTRACT

Lithium evaporation treatments for ATJ graphite tiles in the National Spherical Torus Experiment (NSTX) have shown dramatic improvements in plasma performance increasing the viability of lithium as Plasma Facing Component (PFC) material. In order to understand the complex system of lithiated ATJ graphite, studies of physical and chemical erosion of plain and lithiated ATJ graphite are conducted in the Ion Surface Interaction Experiment (IIAX) facility. Since lithium is known to sputter also as ions, the ionization fraction was measured and found to be 30 ± 6% for a 2000 eV Li ion beam sputtering of lithiated graphite. For chemical erosion measurements, a new facility was developed wherein the target is irradiated with deuterium plasma and the resulting erosion products are detected using a residual gas analyzer. The initial results from this ongoing work are presented here. It is shown qualitatively that lithium treatments suppress the chemical erosion of ATJ graphite.

1. Introduction

Plasma Facing Component (PFC) material choice is one of the most challenging problems faced by the fusion community. Several materials have been considered in the past; however, there is no consensus on the ideal PFC material [1]. While this material research is still ongoing, ITER has proposed to use beryllium as first wall material and tungsten tiles along with carbon fiber composites (CFC) as a diverter material. Carbon based materials are attractive as a PFC material due to its high thermal conductivity, excellent shock resistance, absence of melting and for being a low Z material [2] and ATJ graphite tiles are currently being used in NSTX. However, the chemical erosion of carbon remains a problem. On the other hand, lithium has shown dramatic improvements in plasma performance and suppressing ELMs in NSTX [3] and has the potential as a viable PFC material. In view of the interactions happening between lithium and carbon in NSTX, the current research is aimed at understanding the erosion characteristics of lithiated graphite.

In the past, the Ion Surface Interaction Experiment (IIAX) at the University of Illinois [4–6] has reported studies of thermal evaporation and physical sputtering of ATJ graphite and lithiated ATJ graphite. In this paper, most attention is devoted to chemical erosion measurements of plain and lithiated ATJ graphite. Chemical erosion measurements of ATJ graphite were investigated by several researchers (Meyer et al. [2] and the references there in) earlier and the erosion products monitored were mostly methane (CD_4) and acetylene (C_2D_2). Majority of the previous studies that reported chemical erosion measurements were performed using ion beam irradiation. While this approach greatly simplifies the experiment, it does not reflect the actual conditions seen in tokamaks. To mimic such conditions, a new experimental facility was developed wherein the target material of study is irradiated with low energy plasma. In this paper, the ongoing chemical erosion measurements for plain and lithiated ATJ graphite target when irradiated with low energy deuterium plasma are reported qualitatively. The future work includes measurements of plasma parameters, incident ion flux, and calibrating the residual gas analyzer signals with calibrated leaks.

The experimental setup for chemical erosion measurements is detailed in Section 2 and results along with discussion are presented in Section 3. Finally, summary and conclusions are presented in Section 4.

2. Experimental setup

The experimental setup section consists of two different facilities: one for physical erosion studies and the other for chemical erosion measurements. The experimental setup for physical erosion measurements is already described in previous studies [4–6]. Briefly, an ion beam is used to sputter the target and a quartz crystal microbalance is used to monitor the effects of ion bombardment. For the current work, a 2000 eV lithium ion beam is used to sputter lithiated graphite target for ionization fraction measurements. The details of the experimental setup for chemical erosion are given below.

☆ Work is supported by Department of Energy/ALPS Contract: DEFG02-99ER54515.

* Corresponding and presenting author. Address: 216 Talbot, 104 S. Wright St., Urbana, IL 61801, USA.
E-mail address: vsurla@illinois.edu (V. Surla).

0022-3115/$ - see front matter © 2011 Elsevier B.V. All rights reserved.
doi:10.1016/j.jnucmat.2011.01.051

2.1. Experimental setup for chemical erosion measurements

In the IIAX chamber, the distance between the target and the RGA is large enough that the signal to noise on the RGA makes the chemical erosion measurements difficult. In addition, another goal of the experiment was to look at chemical erosion due to low energy plasma bombardment of the target instead of ion beam irradiation (which is typical of IIAX facility). For this purpose, a new chamber is built for chemical erosion measurements. The key components of this experimental setup are the main chamber and the detection chamber separated by a gate valve as shown in Fig. 1. The main glass chamber consists of an RF antenna coil wound around it for producing RF plasma, a target holder, and a lithium evaporator. The detection chamber consists of a residual gas analyzer for monitoring the partial pressures of all species produced in the main chamber, an ion gauge to calibrate the RGA signals. Each chamber is pumped to low pressures (10^{-7} torr with no gas flow) individually using turbo molecular pump backed by a rough pump. Plasma is produced in the main chamber using RF antenna coil when pressure in the main chamber reaches the mtorr range (with gas flow). In the detection chamber, RGA requires the pressure to be at least in the range of $\sim 10^{-5}$ torr for its operation. This pressure difference is experimentally achieved using differential pumping scheme with three orifices (~2 mm dia. holes) placed in line between the two chambers. With this scheme, the pressure in the detection chamber reaches $\sim 1\text{–}2 \times 10^{-5}$ torr when the gate valve connecting the two chambers is open and when the plasma is on.

Experiments are conducted for three different target configurations (as shown in Table 1):

1. With no target in the main chamber in order to provide a baseline measurement or wall contribution.
2. With ATJ graphite target in the main chamber to study chemical erosion compounds produced.
3. With Li on ATJ graphite to study the effect of lithium treatment on chemical erosion. For this measurement, lithium is in situ evaporated onto graphite using a lithium evaporator.

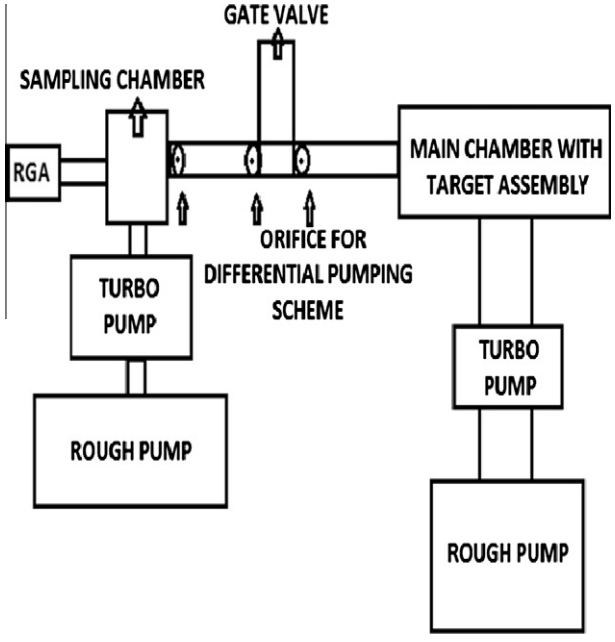

Fig. 1. Schematic of the experimental setup used for chemical erosion measurements. On the left of the diagram is a detection chamber containing RGA. The right chamber is the main chamber that produces plasma–target interactions.

Table 1
List of experiments conducted.

Experiments	Base line (no gas)	No plasma (with gas flow)	Plasma
Case I. No target (wall contribution)	A	B	C
Case II. ATJ target (contribution from graphite + wall)	D	E	F
Case III. Lithiated ATJ graphite (contribution from lithiated graphite + wall)	G	H	I

The experimental approach uses RGA to monitor the partial pressures of selected mass species in 1–65 amu range in the detection chamber. The RGA software allows us to monitor the intensities of selected mass peaks vs. plasma exposure time (P vs. T scans) or alternatively, collecting mass spectra of all species in the range 1–65 amu at a certain given time.

For chemical erosion measurements, the mass spectra are collected after steady state conditions are reached. To obtain steady state, the P vs. T scans for selected mass species were followed until saturation in their intensities occurred. This allows all contributions to the chamber pressure other than the contributions from incident plasma be kept constant during the irradiation runs. Using this approach, the chemical sputtering products are determined by taking differences between mass spectrum from no plasma case and mass spectra acquired during plasma irradiation for the three target configurations described in Table 1 (no target case, ATJ graphite, and lithiated graphite).

In future, the effect of temperature and the energy of incoming ions on chemical erosion of ATJ graphite will be investigated. Temperature dependent measurements are possible by mounting the target on a button heater, which is controlled by a temperature controller. The effect of varying energy will also be investigated by changing the bias on the target.

3. Results and discussion

3.1. Physical erosion measurements

The physical sputtering and thermal evaporation studies of lithiated graphite were reported earlier [4] and the ionization fraction measurements are only an extension to that work. All the experimental conditions used here are similar to the ones described earlier [4]. The motivation to this study comes from the past studies in IIAX where it was found that about two-thirds of lithium comes off as ions for Li, He and D bombardment of lithium [5]. This is described by the secondary ion fraction (or ionization fraction) which is defined as the ratio of secondary ions to the total number of sputtered material. A general question is to find out what is the ionization fraction when lithiated graphite is used as target. The ionization fraction is given as:

$$\text{Ionization fraction} = Y(I)/Y(T) \tag{1}$$

where $Y(I)$ is the sputter-yield contribution from secondary ions and $Y(T)$ is the total sputter yield given by

$$Y(T) = Y(A) + Y(I) \tag{2}$$

where $Y(A)$ is the sputter-yield contribution from neutrals only.

A dual quartz crystal microbalance is used to measure the sputter yields similar to our previous studies [4]. In a typical experiment, the total sputter yield, $Y(T)$ is measured with QCM. However, to determine the ionization fraction, the target is negatively biased such that the sputtered ions fall back to the target. Typically, the energy distribution of sputtered particles is in the

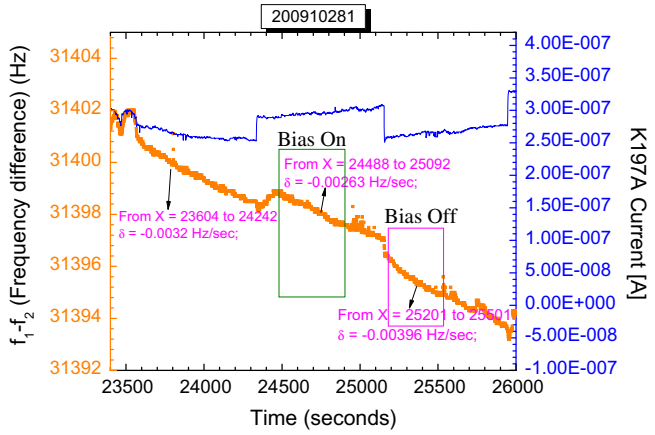

Fig. 2. Typical QCM data for sputtering measurement showing change in frequency with change in bias. The frequency changes of QCM and the ion current are plotted together. The boxes represent the region in which slopes are computed.

order of few eV and so, a small bias voltage is sufficient to collect majority of the secondary ions sputtered from the target. To determine this bias voltage required, the applied voltage on the target is varied until the target current reading saturates and it was found that a negative bias of 30 V is sufficient. In the case of negatively biasing target, the QCM measures only the sputter-yield contribution due to neutrals alone and therefore, $Y(A)$ is measured. Subtracting $Y(A)$ from $Y(T)$, $Y(I)$ can be obtained from which the ionization fraction is computed. Fig. 2 shows the QCM data for a 2000 eV lithium ion beam striking the lithiated graphite target in which the frequency changes of QCM and the ion current are plotted together. The frequency difference, f_1–f_2, is the net frequency change obtained after subtracting the baseline in dual QCM method [5]. The change in the slope of QCM represents the amount of sputtered material deposited. As shown in Fig. 2, the QCM slopes are changed due to "bias off" and "bias on" conditions which represent the signal corresponding to $Y(T)$ and $Y(A)$ respectively. The boxes in Fig. 2 represent the region in which slopes are obtained, from which sputter yields can be calculated [5]. This results in an ionization fraction value of 30 ± 6%. The error on the measurement is due to variation in QCM slopes at different iterations. The ionization fraction value of 30% for lithiated graphite target is lower than the reported value of 66% for lithium target [5], which may be explained by the influence of oxygen. It is known from earlier studies that the presence of oxygen or other electronegative species at the surface increases secondary ion yields [7]. So, in the pure lithium case, owing to its high reactivity, it is possible that lithium is covered with a monolayer of lithium oxide on the surface resulting in a high secondary ion fraction. However, in the Li–C system, there are relatively fewer Li–O bonds on the surface. In addition, carbon is less electronegative than oxygen as well which may have led to a decrease in the observed ionization fraction.

3.2. Chemical erosion measurements

All the experiments shown in Table 1 are conducted to monitor the chemical erosion products due to contribution from wall, ATJ graphite target and lithiated graphite target. The working gas used for producing plasma is deuterium. The mass spectra were collected after steady state conditions have reached for each of the experimental runs shown in Table 1. The baseline scans are conducted in order to compare experiments done on different days. For example, runs A, B and C are done on 1 day and D, E, and F are done on another day after loading the ATJ graphite in the target. While efforts are taken to mimic the same gas flow conditions

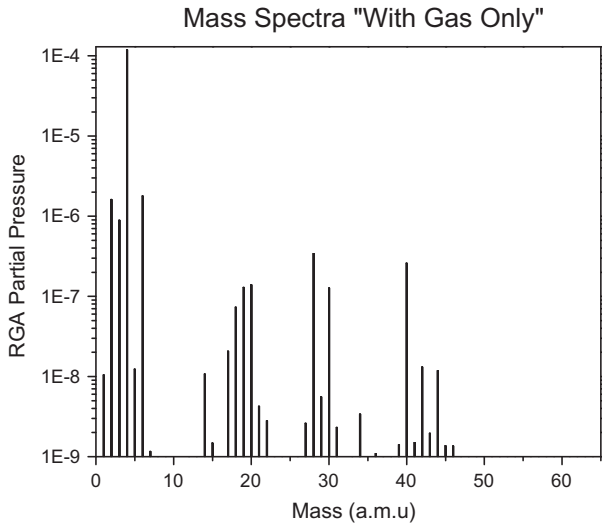

Fig. 3. Mass spectra obtained after subtracting the baseline (no gas flow) for ATJ graphite case when there is no plasma (run 'E'–run 'D' from Table 1).

for each run day, runs A and D might be slightly different. In order to allow any comparisons to be made for different experimental runs, the baseline scans are collected for all the cases. The baseline scans (A, D, and G) are generally subtracted from the subsequent gas only case and plasma case conducted on the same day. Fig. 3 shows a mass spectra for ATJ graphite obtained after subtracting the baseline (run 'E'–run 'D') for the no plasma case. As can be seen from Fig. 3, the dominant peak is due to deuterium gas at mass 4. Fig. 4 shows a plasma irradiated mass spectra for ATJ graphite obtained after subtracting the baseline (run 'F'–run 'D'). Now, the chemical sputtering products can be determined by taking differences between the mass spectrum for no plasma case (in Fig. 3) and mass spectra acquired during plasma irradiation (in Fig. 4). This subtraction (run 'F'–run 'E') results in mass spectra for ATJ graphite as shown in Fig. 5, which represents the true contribution of the plasma to chemical erosion. In Fig. 5, three distinct groups of masses can be seen: (1) in the mass range 12–20 amu, (2) in the mass range 26–32 amu, and (3) in the mass range 40–44 amu. In this paper, for simplicity, only single carbon chain products are in-

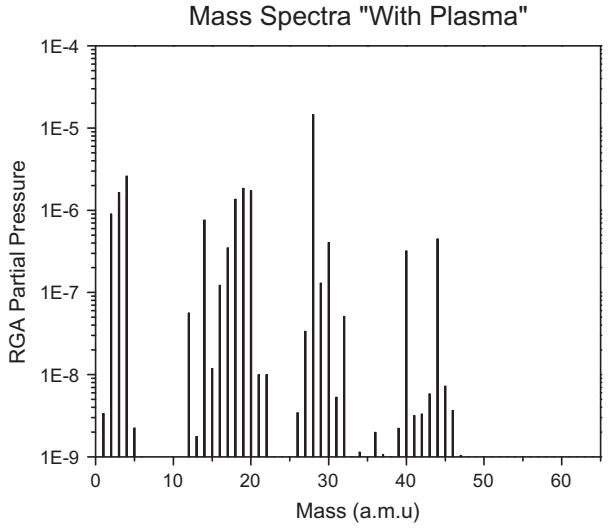

Fig. 4. Mass spectra obtained after subtracting the baseline for ATJ graphite case when the plasma is ON (run 'F'–run 'D' from Table 1).

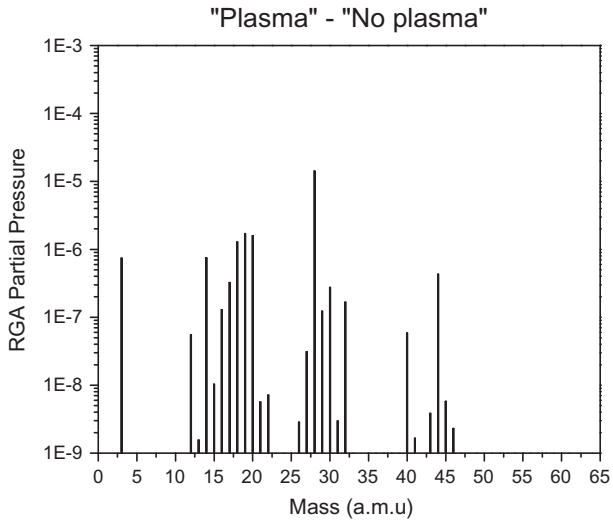

Fig. 5. Mass spectra obtained after subtracting the "no plasma" case from "plasma" case (run 'F'- run 'E' from Table 1). This represents the actual contribution of the plasma to chemical erosion.

cluded by which the analysis is limited to the first group of peaks in the range 12–20 amu. The single carbon erosion products include CD_4, CD_3H, CD_2H_2, CDH_3 and CH_4. However, as the percentage of deuterium is much higher than hydrogen in the current experimental chamber, the higher isotopic exchange products are ignored and we limit to cases where only one substitution of deuterium with hydrogen is allowed. Thus, the chemical erosion species considered in the current analysis are CD_4 and CD_3H. In addition, the peaks in mass range 16–20 amu have contributions from H_2O, HDO, and D_2O. Each mass signal may have contribution based on the cracking pattern of the species. For example, CD_4 (mass 20) cracks into CD_3 (18), CD_2 (16) and CD(14) in a ratio of 0.9999:0.8888:0.2040:0.1070. There are five unknows (CD_4,CD_3H, H_2O, D_2O, HDO) in the mass range 16–20 amu and in the current analysis, only signals from S_{16} to S_{20} are considered. The resulting five equations due to S_{16}–S_{20} signals can be written as follows:

$$S_{16} = 0.2040P_{CD_4} + 0.1020P_{CD_3H}$$

$$S_{17} = 0.444P_{CD_3H} + 0.1060P_{HDO} + 0.2120P_{H_2O}$$

$$S_{18} = 0.8888P_{CD_4} + 0.444P_{CD_3H} + 0.1060P_{HDO} + 0.2120P_{D_2O} + 0.9999P_{H_2O}$$

$$S_{19} = 0.9999P_{CD_3H} + 0.9999P_{HDO}$$

$$S_{20} = 0.9999P_{CD_4}0.9999P_{D_2O}$$

The above five equations can also be represented by the following equation

$$S_j = \sum_i M_{ij} * P_i$$

where S_j correspond to the signal at mass 'j' (j = 16, 17, . . . , 20 in the current study) due to true contribution of the plasma and P_i denotes the partial pressure of species 'i'. For example, S_j for the masses 16–20 amu can be obtained from Fig. 5. The coefficients, M_{ij}, correspond to the contribution from species 'i' on signal 'j', which are obtained from cracking patterns [8]. Since S_j and M_{ij} are known, one could solve for P_i. Solving the above set of five equations for five unknowns, the partial pressures (P_i) of all the species considered here are determined. Note that the inclusion of higher order hydrocarbon chain species will complicate the analysis as the equations corresponding to the second group (26–32 amu) and their cracking patterns should also be included.

Using the simple aforementioned mathematical approach, the partial pressures P_{CD_4}, P_{CD_3H}, P_{H_2O}, P_{HDO}, and P_{D_2O} are obtained for all the three experimental cases described in Table 1. These results are summarized in Fig. 6. It can be seen that majority of the contribution is coming from the chamber walls alone which is marked by circles in Fig. 6 (case I in Table 1). And, secondly there is lot of D_2O and HDO present in the chamber compared to the amount of CD_4 and CD_3H. While this indicates that deep cleaning is required for future measurements to minimize wall contributions, the high amounts of D_2O and HDO in the current measurement could be attributed to pre-lithium conditions existing on the chamber walls. Pre-lithium conditions correspond to any passivated lithium present on the chamber walls from previous experimental runs. For e.g., deuterated lithium hydroxide (Li-OD) present on the chamber walls may give off OD to form D_2O when deuterium plasma comes in contact with the wall.

Fig. 6 also shows results from ATJ graphite (case II in Table 1), which are represented by diamonds. Firstly, it can be seen that the signals of CD_4 and CD_3H in case II are higher compared to the the bare wall case, which is due to the chemical erosion of ATJ graphite. Secondly, the amount of D_2O, HDO and H_2O remained almost same in both cases. The minor differences in the signals could be attributed to different experimental conditions existing in the chamber while inserting ATJ graphite into the chamber.

The results of lithiated graphite target (case III in Table 1) are also shown in Fig. 6, which are marked by triangles. First, it can be seen that the CD_4 and CD_3H signals from lithiated graphite are lower than ATJ graphite. Thus qualitatively, it can be concluded that lithium treatment suppresses chemical erosion of graphite. Secondly, it can be seen that the signals from D_2O and HDO are also suppressed. As lithium is evaporated in situ onto ATJ graphite target, some lithium is also deposited on the walls of the chamber and this fresh lithium is believed to be the reason for suppressing the contribution of D_2O and HDO coming from the walls. This is intriguing result in that a fresh lithium coating suppresses D_2O and HDO signals while passivated lithium resulted in an increase in D_2O and HDO. Additional experiments are underway to test this hypothesis by taking off the lithiated graphite target from the

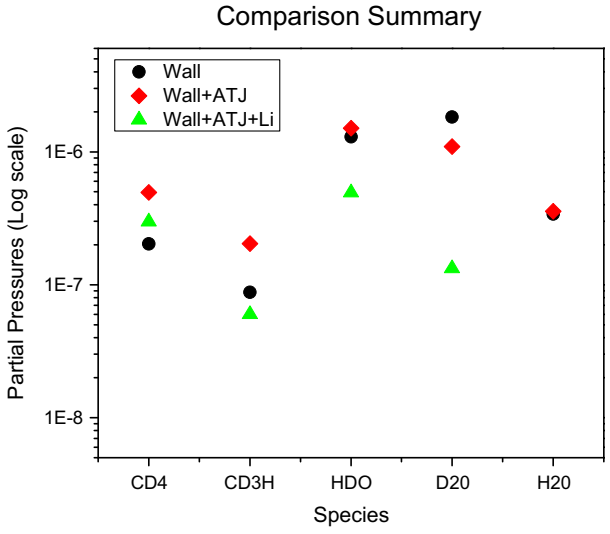

Fig. 6. Comparison of partial pressures of the considered species for three different experimental conditions namely (1) wall (with no target) represented by circles, (2) wall + ATJ (with ATJ graphite target) represented by diamonds, and (3) wall + ATJ + Li (With lithiated ATJ graphite) represented by triangles.

chamber (similar to case I but with modified walls as lithium is redepoisted on some region of the walls). Additionally, the amount of water stays the same for both case I and case II (overlapped in Fig. 6), however, for case III when lithium is present in the chamber, the solution yielded that H_2O peak be negative (not shown in Fig. 6) indicating that lithium getters water vapor.

4. Summary and conclusions

Erosion studies of lithiated graphite are conducted in IIAX. While the physical sputtering and evaporation studies were reported earlier, this work reports the ionization fraction to be 30% for sputtering of lithiated graphite by 2000 eV lithium ions. A new facility is built for chemical erosion measurements based on residual gas analyzer. In the current study, the species considered are CD_4, CD_3H, D_2O and HDO and for analysis, a simple mathematical approach is presented. It was found that D_2O and HDO are present in relatively huge amounts compared to the expected chemical erosion products (CD_4 and CD_3H). While this requires further investigation, these could be due to the contribution from the walls from pre-existing lithium conditions. However, fresh lithium evaporation has resulted in suppressing D_2O and HDO signals demonstrating the beneficial effects of lithium. Further, lithium treatments to ATJ graphite have shown to suppress the chemical erosion products considered here.

More detailed experiments are being planned for future chemical erosion measurements. These involve deep cleaning the chamber to minimize the wall contribution and incorporating a bigger target to increase the chemical erosion products. Also, ex situ evaporation of lithium onto ATJ graphite is being considered to minimize the lithium depositing on the walls. The goal is to obtain absolute chemical erosion sputter yields for plasma irradiation of lithiated ATJ graphite.

Acknowledgements

This work is supported by DOE Contract DE-FG02-04ER54765. The authors would like to thank Dr. M. Neito and Dr. M. Jaworski for technical discussions, S. Jung for his assistance with RF plasma, and undergraduates J. Peck and T. Pixton for their help with the experiment.

References

[1] M. Greenwald, Priorities, Gaps and Opportunities, Report to the Fusion Energy Sciences Advisory Committee, October 2007.
[2] F.W. Meyer, H.F. Krause, L.I. Vergara, J. Nucl. Mater. 337–339 (2005) 922–926.
[3] H.W. Kugel, D. Mansfield, the NSTX team, J. Nucl. Mater. 390-39 (2009) 1000–1004.
[4] Kenzo Ibano, Vijay Surla, David N. Ruzic, IEEE Trans. Plasma Sci. 38 (3) (2010).
[5] J.P. Allain, D.N. Ruzic, Nucl. Fusion 42 (2002) 202–210.
[6] M. Racic, K. Ibano, R. Raju, D.N. Ruzic, J. Nucl. Mater. 390-39 (2009) 1043–1047.
[7] Peter Williams, Surf. Sci. 90 (1979) 588–634.
[8] M. Nieto-Perez, J.P. Allain, C.B. Heim, C.N. Taylor, J. Nucl. Mater., (2010), in press.